AIP | Journal of Applied Physics

Thermal conduction in nano-porous silicon thin film

G. H. Tang, C. Bi, and B. Fu

Citation: Journal of Applied Physics **114**, 184302 (2013); doi: 10.1063/1.4829913
View online: http://dx.doi.org/10.1063/1.4829913
View Table of Contents: http://scitation.aip.org/content/aip/journal/jap/114/18?ver=pdfcov
Published by the AIP Publishing

Thermal conduction in nano-porous silicon thin film

G. H. Tang,[a] C. Bi, and B. Fu
MOE Key Laboratory of Thermo-Fluid Science and Engineering, School of Energy and Power Engineering, Xi'an Jiaotong University, Xi'an 710049, China

(Received 24 September 2013; accepted 26 October 2013; published online 12 November 2013)

Controlling the thermal conductivity of thermoelectric materials continues to be a goal for energy conversion applications. The Phonon Boltzmann Transport Equation is solved by using the Discrete Ordinates Method to numerically study the phonon thermal conductivity of nano-structured silicon thin film with pores in this study. The effects of the film thickness, film porosity, and porous structure are concerned. The numerical results show that the nano-pores are able to reduce the thermal conductivity of the silicon thin film sharply by the phonon boundary scattering, and the scattering boundary area has significant effect on the thermal conductivity. The method of local angle distribution between heat fluxes is introduced for the first time to optimize the pore placement for reducing the thermal conductivity. © *2013 AIP Publishing LLC*.
[http://dx.doi.org/10.1063/1.4829913]

I. INTRODUCTION

The thermoelectric materials have been attracting increasing attention recently due to their ability of converting heat into electricity.[1–6] The efficiency of thermoelectric devices can be described by the dimensionless thermoelectric figure of merit $ZT = \sigma S^2 T/\lambda$, where σ is the electrical conductivity, S is the Seebeck coefficient, T is the temperature, and λ is the thermal conductivity.[7] To improve the performance of the thermoelectric devices, we can independently optimize the thermal conductivity and electrical conductivity due to different size effects with respect to phonons (carry heat) and electric charges (carry current).[8–10] Phonons are remarkably scattered at boundaries and interfaces in nanostructure size, which leads to a decrease in thermal conductivity, while the electrical conductivity is less sensitive to a decrease in nanostructure size.[11] We can take advantage of the phonon scattering on boundaries to reduce the thermal conductivity for high performance of thermoelectric devices. Existing studies[12–17] suggested that nano-porous thin films can block heat transfer easily, and result in thin films with low thermal conductivity. However, the experimental study is often constrained by the nanofabrication due to the nano-scale, and high measurement accuracy of experimental system is often difficult to achieve and the cost is expensive as well. Numerical simulation is a good tool to make up for the limitation of the experimental study. Many numerical studies focus on the size effect (film thickness and pore size) on the thermal conduction in the nano-porous thin film with uniformly arranged pores, but few have studied the effects of the porosity and scattering boundary area (or specific surface area). In addition, once the nano-pores are non-uniformly arranged, the heat conduction in thin film will exhibit differently, but few studies have reported on it, and optimizing pore placement in film for further reducing the thermal conductivity is also investigated rarely. Therefore, it is quite necessary to study the effect of the pore placement and the optimization method on the thermal conduction in the nano-porous thin film.

The Phonon Boltzmann Transport Equation (PBTE) is widely employed to study the thermal conductivity of nano-structured materials. In the present study, we solve the two-dimensional PBTE to study the thermal conductivity of silicon thin film with nano-pores. We focus on the effects of the porosity, film thickness, and surface area of the boundary on the effective thermal conductivity, in order to reduce the thermal conductivity of silicon thin film further. The basic theory of phonon transport as well as the method of solving the PBTE is described in Sec. II. In Sec. III A, we employ analytical solutions and available numerical results to verify the present numerical method. In Sec. III B, the effects of film porosity, film thickness, and scattering boundary area are studied. In Sec. III C, the relation between heat flux and thermal conductivity is discussed and the thermal conduction in the thin film with non-uniformly arranged pores is investigated. A brief conclusion is presented in Sec. IV.

II. METHODOLOGY

A. Phonon Boltzmann transport equation

The Boltzmann Transport Equation (BTE) describes well the transport of basic particles, such as dilute gas molecules, electrons, photons, and phonons. As there is no external force, the BTE is expressed as[8,18]

$$\frac{\partial f(\mathbf{r},\mathbf{v},t)}{\partial t} + \mathbf{v}\cdot\nabla f(\mathbf{r},\mathbf{v},t) = \left(\frac{\partial f(\mathbf{r},\mathbf{v},t)}{\partial t}\right)_s, \quad (1)$$

where, f is the distribution function, t is the time, $\mathbf{v}$ is the velocity vector of the particles, and $\mathbf{r}$ is the position vector. The right hand is the scattering term, and is often in the relaxation-time approximation as

$$\left(\frac{\partial f}{\partial t}\right)_s = -\frac{f - f_0}{\tau(\mathbf{r},\mathbf{p})}, \quad (2)$$

[a]Author to whom correspondence should be addressed. Electronic mail: ghtang@mail.xjtu.edu.cn. Tel.: +86-29-82665319. Fax: +86-29-82665445.

where, f_0 is the local equilibrium distribution function, τ is the relaxation time, and $\mathbf{p}$ is the momentum. For phonons, using the concept of phonon intensity[19,20]

$$I(p,\omega,\mathbf{r},\mathbf{s},t) = v(p,k)f\hbar\omega(p,k)D(\omega), \tag{3}$$

and multiplying Eq. (1) by $v\hbar\omega D(\omega)$, we can obtain the PBTE

$$\frac{1}{v}\frac{\partial I}{\partial t}+\cos\theta\frac{\partial I}{\partial x}+\sin\theta\cos\varphi\frac{\partial I}{\partial y}+\sin\theta\sin\varphi\frac{\partial I}{\partial z}=-\frac{I-I_0}{v\tau(p,\omega,T)}. \tag{4}$$

In Eqs. (3) and (4), $v(p, k)$ is the group velocity of phonon branch p and wave vector k, $\hbar$ the Reduced Planck's constant, ω the angular frequency of phonons, D the density of states given by $D = k^2/2\pi^2 v$, $\tau(p,\omega,T)$ the phonon relaxation time, and $\mathbf{s}$ the unit vector of phonon transport direction, i.e., $\mathbf{s} = (\cos\theta, \sin\theta\cos\varphi, \sin\theta\sin\varphi)$, where, θ is the polar angle, φ is the azimuthal angle, as schematic in Fig. 1. In addition, I_0 denotes the local equilibrium intensity, and obeys Bose-Einstein statistics[8]

$$I_0(p,\omega,T) = \frac{1}{4\pi}\frac{v\hbar\omega D}{\exp(\hbar\omega/k_BT)-1}. \tag{5}$$

To solve Eq. (4), we first need to obtain the parameters of ω, v, and τ. A simple assumption is the gray model (single average phonon mean free path without frequency dependence), but it will overestimate the thermal conductivity of the nano-structured silicon.[21] To obtain accurate results, we should incorporate the frequency dependence of relaxation time and the phonon group velocity. The relation between ω, k, and v can be obtained from the phonon dispersion, and we can also obtain τ from Molecular Dynamics Simulations[22] or the First Principle solutions.[23]

In the present study of silicon film, we consider: (1) The heat conduction is in steady-state in the film. (2) The maximum wave vector is in the first Brillouin zone, given by $k_{max} = 2\pi/a$, where $a = 5.43$ Å denotes the lattice constant of the silicon. Only two transverse acoustic (TA) and one longitudinal acoustic (LA) branches are considered, since the optical phonon branches have low contribution to the thermal conduction at room temperature.[8] The phonon transport in the silicon film is isotropic, and the (100) lattice direction phonon dispersion is used to calculate the frequency-dependent group velocity. Here, we choose Pop's relation to calculate the frequency of the bulk silicon[24]

$$\omega = \omega(p,k) \approx \omega_0 + v_s k + ck^2, \tag{6}$$

and group velocity $v = \partial\omega/\partial k = v_s + 2ck$, where, v_s and c are coefficients, for TA: $v_s = 5230$ m/s, $c = -2.26\times10^{-7}$ m^2/s; and for LA: $v_s = 9010$ m/s, $c = -2.00\times10^{-7}$m^2/s. (3) The total phonon relaxation time is estimated by Matthiessen's rule from the impurity scattering, Normal process and Umklapp process, given by $\tau^{-1} = \tau_i^{-1} + \tau_N^{-1} + \tau_U^{-1}$. The impurity scattering relaxation time is solved by $\tau_i^{-1} = A\omega^4$, where $A = 1.32\times10^{-45}$s^3 according to Asheghi *et al.*[25] To simplify the calculation, we use the Henry' relation to solve the relaxation time by combining the Normal process and Umklapp process, given by $\tau_{N+U} = A_{NU}(\omega/2\pi)^{-2}T^{-b}$, where $A_{NU} = 5.32\times10^{18}K^{1.49}$/s, $b = 1.49$ for LA phonons; and $A_{NU} = 5.07\times10^{18}K^{1.65}$/s, $b = 1.65$ for TA phonons.[22]

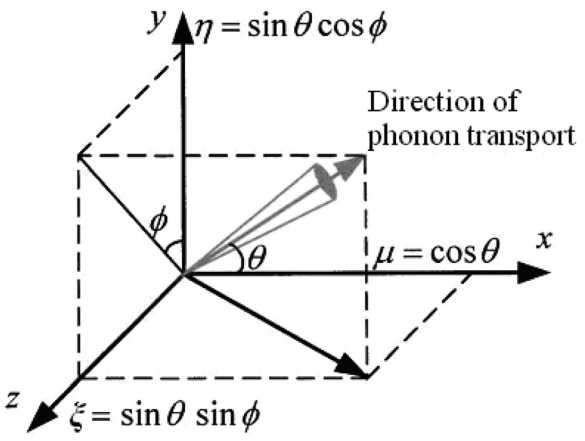

FIG. 1. Coordinate system of the phonon Boltzmann equation simulation.

B. Method of numerical solution

Equation (4) is similar to the thermal Radiative Transport Equation (RTE).[19,26] We can use the method of solving RTE to solve Eq. (4). The widely used method is the Discrete Ordinates Method (DOM).[27] The DOM is based on a discrete representation of the directional variation of the radiative intensity, which transforms the equation of radiative transfer into a set of simultaneous partial differential equations. A solution to the transport problem is found by solving the equation of radiative transfer for a set of discrete directions spanning the entire solid angle 4π. The integrals over the solid angle are approximated by numerical quadrature. In this study, we choose the higher order S_8 quadratures compared with S_4 used in Ref. 28 and finer meshes over 100×100 compared with 31×31 used in Ref. 16 to reduce the false scattering and ray effect.

Once the phonon intensities of each direction $I(p,\omega,\mathbf{r},\mathbf{s})$ is obtained by solving Eq. (4), the frequency-dependent equilibrium intensity can be calculated by the numerical integration over the total solid angle 4π. For S_N quadratures, we have

$$I_0(p,\omega,\mathbf{r}) = \frac{1}{4\pi}\sum_{i=1}^{n} w_i I_i(p,\omega,\mathbf{r},\mathbf{s}), \tag{7}$$

where i is the discrete direction index, n the total directions, and w_i the quadrature weights associated with the ith direction. Then, integrating Eq. (7) over the phonon frequency and branch, we obtain the total equilibrium intensity

$$I_0(\mathbf{r}) = \sum_p \int_0^{\omega_{max}} I_0(p,\omega,\mathbf{r})d\omega. \tag{8}$$

For heat flux, firstly we integrate $I(p,\omega,\mathbf{r},\mathbf{s})$ over the phonon frequency and branch to obtain the total intensity,

and then the heat flux at each node can be calculated by the S_N quadratures

$$\mathbf{q}(\mathbf{r}) = \sum_{i=1}^{n} w_i \mathbf{s}_i \sum_p \int_0^{\omega_{\max}} I_i(p, \omega, \mathbf{r}, \mathbf{s}) d\omega. \quad (9)$$

In nanoscale, the temperature cannot be defined as a measure of equilibrium, but we can use the effective temperature to reflect the local energy density. We can solve Eqs. (5) and (8) based on the energy conservation to obtain the effective temperature, where the energy conservation is expressed as

$$I_0(\mathbf{r}) = \sum_p \int_0^{\omega_{\max}} I_0(p, \omega, \mathbf{r}) d\omega = \sum_p \int_0^{\omega_{\max}} \frac{1}{4\pi} \frac{v\hbar\omega D}{\exp[\hbar\omega/k_B T(\mathbf{r})] - 1} d\omega. \quad (10)$$

C. Boundary condition

The scattering boundary resulted from the phonons collision with the boundaries, is the most common boundary condition for solving the PBTE, given by[29]

$$I(\mathbf{r}_w, \mathbf{s}) = pI(\mathbf{r}_w, \mathbf{s}') + (1-p)\frac{1}{\pi} \sum_{i=1, \mathbf{n}\cdot\mathbf{s}<0}^{n} w_i I(\mathbf{r}_w, \mathbf{s}) |\mathbf{n} \cdot \mathbf{s}|, \quad (11)$$

where, p is the boundary specularity depending on the boundary roughness and phonon wavelength,[8] $\mathbf{n}$ the inward-facing normal vector of the boundaries, $\mathbf{r}_w$ the position coordinates of the boundaries, and $\mathbf{s}'$ the direction associated with $\mathbf{s}$ by specular reflection on the boundaries. We have symmetry boundaries for $p = 1$ while completely diffuse boundaries for $p = 0$. The second term of the right-hand of Eq. (11) denotes the diffuse scattering reflection.

III. RESULTS AND DISCUSSION

A. Validation of numerical method

In this section, two examples are used to validate the present numerical method. The first example is the validation of the cross-plane thermal conductivity of pure silicon thin film. Both the gray model and frequency-dependent model are compared with the Majumdar's relation[19] and Sellan's numerical results,[30] respectively. We solve the two-dimensional PBTE by treating the top and bottom boundaries as symmetry boundaries to simulate the thermal conduction in the thin film, and treating the left and right boundaries as "phonon black body emission,"[29] see Fig. 2(a). The average heat flux across the thin film can be calculated by

$$\overline{q_x}(x) = \frac{1}{Y} \int_0^Y q_x(x, y) dy, \quad (12)$$

where Y is the height of the computational zone. In Fig. 2(a), the symmetry boundary (specular reflected boundary condition of $p = 1.0$) ensures a constant heat flux, i.e., $\overline{q_x}(x) = \text{const}$,

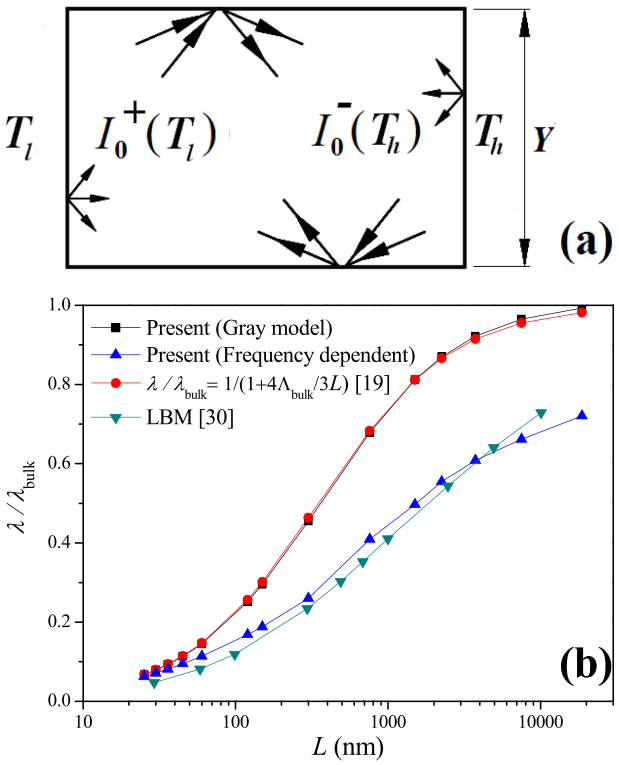

FIG. 2. Validation of the present numerical method for predicting the cross-plane thermal conductivity of the pure silicon film. (a) Boundary conditions of pure thin film. (b) Comparison between the present predictions and the published data.

so the effective thermal conductivity of the thin film can be calculated from Fourier's Law as

$$\lambda = \frac{\overline{q_x}}{(T_h - T_l)} L, \quad (13)$$

where, T_h and T_l are the temperature at the two sides of the thin film, respectively, and L is the thin film thickness in the x direction. Here, we set T_h and T_l to be 295 K and 293 K, respectively. Fig. 2(b) presents the comparison between the numerical results and available data. We can see that the present Gray model is in perfect agreement with the Majumdar's relation, which proves that using DOM with the S_8 quadratures in this study can solve the PBTE accurately. From the comparison between the present frequency-dependent model and the Sellan's results, although some deviations can be found, we can still believe that these two methods are in good agreement. Here, the deviations are inevitable, since the solving methods of PBTE between DOM and Lattice Boltzmann Method (LBM) are different, and the used phonon dispersion curves are also different. Based on the above analysis, we believe that the present frequency-dependent model is of enough accuracy to predict thermal conductivity of the thin film. In addition, we can also find that the Gray model overestimates the thermal conductivity too much, especially for the film thickness over 100 nm.

The second example is to validate the present numerical method for the nanoporous thin film. In the simulation, all the conditions are the same as those in Hao's Monte Carlo simulation (MC).[21] The structure of the nanoporous thin film

is shown in Fig. 3(a)), and a period unit cell is chosen for the study. The porosity in Fig. 3(a) is defined as $\Phi = D^2/L^2 = 0.25$, where D is the pore size and L is the length of the unit cell. All phonons scattering on the rough pore boundaries are set to be diffuse reflection, i.e., $p = 0$ in Eq. (11). On the four edges of the unit cell we set periodic boundary condition, for example, in the x-direction we have

$$I(p,\omega,x=0,y,s) - I_0(p,\omega,x=0,y,s) = I(p,\omega,x=L,y,s) - I_0(p,\omega,x=L,y,s). \quad (14)$$

Since the diffuse reflection on the pore boundaries can lead to the reduction of the phonon intensity, the average heat flux $\overline{q_x}(x)$ is no longer a constant, and the effective heat flux should be re-averaged over the whole porous media. For Fig. 3(a), the heat flux is given by

$$\overline{q_x} = \int_0^L \overline{q_x}(x)dx = \frac{1}{L^2}\int_0^L\int_0^L q_x(x,y)dydx, \quad (15)$$

and then the effective thermal conductivity of the porous thin film should be solved by Eqs. (13) and (15). Fig. 3(b) plots the predicted thermal conductivity of the nanoporous silicon film. The present predictions are in good agreement with Hao's MC results. Those slight deviations can be ascribed to the difference between the bulk Si dispersion and porous Si dispersion (In this study, we use the bulk Si dispersion for approximation). In addition, the difference between the solving methods of DOM and MC will also result in deviations. Therefore, the above analysis confirms that the present method can also be used to predict the thermal conductivity of the nanoporous thin film.

B. Effective thermal conductivity of nano-porous silicon thin film

With the development of nanofabrication, experimental studies mostly focused on the ordered nano- and mesoporous thin films.[12,15,31,32] According to Ref. 33, the pore shape has less effect on the thermal conductivity when porosity <0.4 or film thickness >100 nm at higher porosity, so in the following work we employ the ordered nano-porous thin film with square pores, and the pore shape is shown in Fig. 4(a). Due to the size effect resulting from the film thickness, both the in-plane and cross-plane thermal conductivities are investigated. For the in-plane thermal conductivity (y direction), the boundary conditions of film edges AD and BC are set to be diffuse reflection, and we use the periodic boundary conditions for AB and CD edges. For cross-plane thermal conductivity (x direction), AD and BC edges are phonon black body emission which can be given by Eq. (5), and symmetry boundary (specular reflected boundary condition of $p = 1.0$) is set for AB and CD edges. The porosity in Fig. 4(a) is also defined as $\Phi = D^2/L^2$, and all the pore boundaries are diffuse reflection for phonon scattering. The thermal conductivity is calculated by Eqs. (13) and (15).

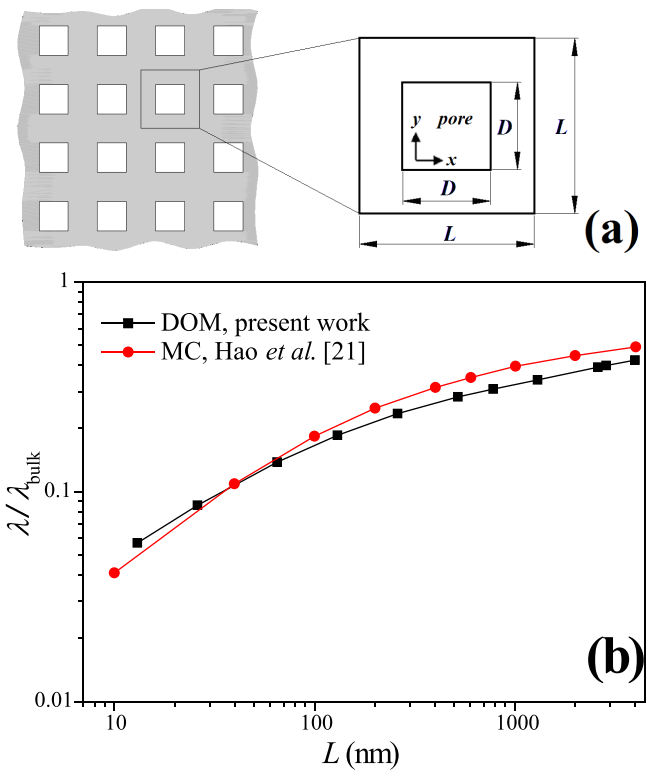

FIG. 3. Validation of the present method for predicting the thermal conductivity of the porous silicon film. (a) The structure of the porous silicon film. (b) Comparison between the present predictions and MC results.

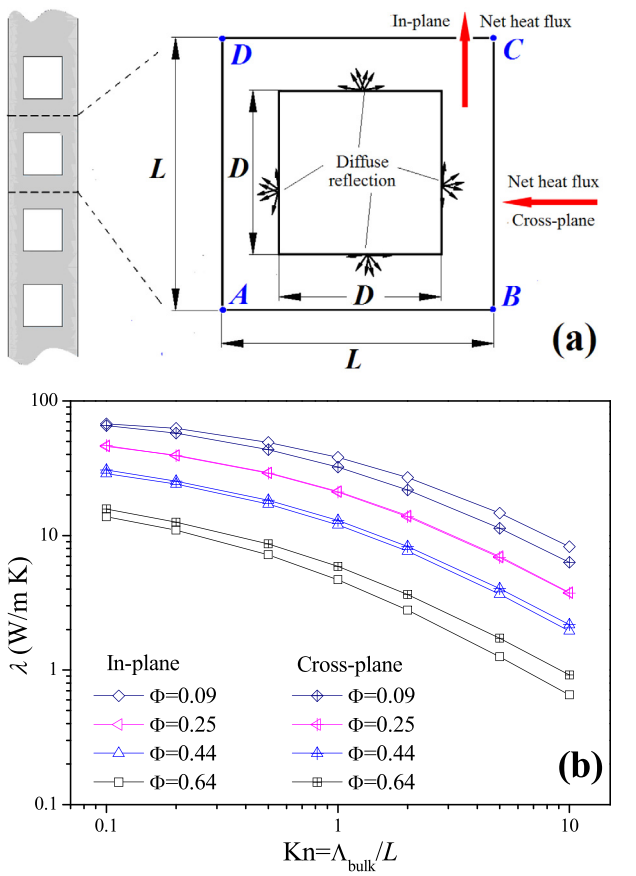

FIG. 4. Effects of the porosity and film thickness on the thermal conductivity of the silicon film. (a) Schematic of nano-porous silicon thin film. (b) Thermal conductivity of the porous silicon film ($p = 0$).

Figure 4(b) shows the effects of the porosity and film thickness on the thermal conductivity of the silicon film, where the thickness of the film is normalized by the bulk silicon mean free path, which can be estimated from $\lambda_{bulk} = 1/3C_V v\Lambda_{bulk}$ with the volume specific heat C_V and average phonon group velocity v. We have $\Lambda_{bulk} \approx 260$ nm from the corresponding parameters in Ref. 26. From Fig. 4(b), we can see that as the porosity increases (by increasing the pore scale D), the effective thermal conductivity gets lower, because the increase of Φ will lead to the decrease of the solid zone and thus the increase of the scattering boundary area. The size effect is also important. With the increase of Kn, the size effect will be more significant, and the thermal conductivity can be reduced sharply compared with the bulk value of 150 W/(m K). For example, the porous thin film with $Kn = 10$ and $\Phi = 0.25$ has a low thermal conductivity of about 3.8 W/(m K), which is reduced by two orders in magnitude compared with the bulk value. Also, we can get an extremely low thermal conductivity by continuing to increase the porosity up to 64%.

In addition, the porosity also has effect on the thermal conduction in different directions. From Fig. 4(b), we can see that the in-plane thermal conductivity (λ_{in}) is higher than the cross-plane thermal conductivity (λ_{cross}) at $\Phi = 0.09$, and with the increase of the porosity until $\Phi = 0.25$, we have $\lambda_{in} \approx \lambda_{cross}$. If we continue to increase the porosity Φ, we have $\lambda_{in} < \lambda_{cross}$. This phenomenon can be attributed to the different boundary conditions between the in-plane and cross-plane cases. First, in the pure thin film we have $\lambda_{in} > \lambda_{cross}$. Once we open small pores in the pure thin film, at low porosity (for $\Phi < 0.25$ in this study) the pore boundary has little effect on the phonon scattering, which cannot reduce the phonon intensity significantly, so we still keep $\lambda_{in} > \lambda_{cross}$. When $\Phi > 0.25$, the pore boundary area will be expanded so much that the phonons have more chance to collide with the boundary, resulting in sharp reduction of the phonon intensity. Second, only the diffuse reflections can reduce the phonon intensity instead of the specular reflection and periodic boundary. Along the net heat flux direction, see Fig. 4(a), the diffuse boundaries are the boundaries of AD, BC and the pore wall for the in-plane case, while the pore wall only is the diffuse boundary for the cross-plane case. This denotes that the in-plane case has larger diffuse scattering boundary area, which can reduce the phonon intensity more significantly, and then result in $\lambda_{in} < \lambda_{cross}$ for $\Phi > 0.25$.

Romano *et al.*[17] reported that the boundary specularity (p in Eq. (11)) has significant effect on the thermal conductivity of low porosity (5%–30%) thin film when the pore size is comparable to the phonon mean free path. In the present study, we will study the effect of the pore boundary specularity on the thermal conductivity within a wider range of porosity 9%–64%, and the results are shown in Fig. 5. We can see that the thermal conductivity increases with the increase of p, because lower specularity can disorder the phonon transport more easily.[15] In low porosity film ($\Phi = 9.0\%$), the effect of p can be neglected. But as the porosity increases, the effect of the boundary specularity becomes important increasingly, and the thinner of the film (denotes larger Kn), the more important effect of p. In high porosity film

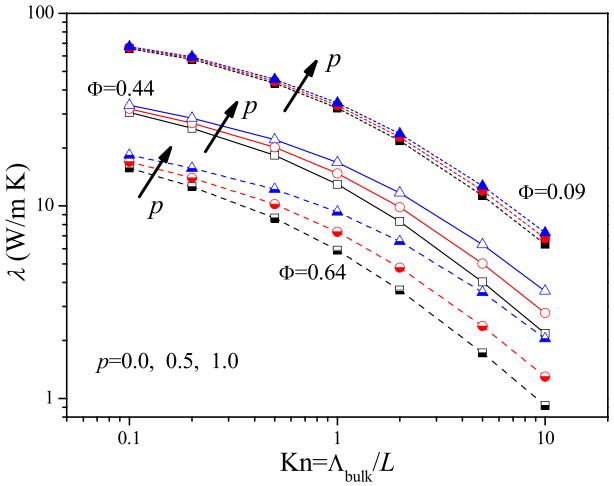

FIG. 5. Effect of boundary specularity on effective thermal conductivity (cross-plane).

($\Phi = 64\%$), the effect of p cannot be neglected even if the film thickness are ten times of the bulk phonon mean free path (about 260 nm). We can conclude that the rough boundaries reduce the thermal conductivity significantly in high porosity film while the influence is small in low porosity film, because high porosity is usually accompanied by a large specific surface area, which leads to more boundary area for phonon scattering. From the above analysis, we can indirectly find that the specific surface area or the boundary area of the pores has an important effect on the thermal conductivity as well, but Fig. 5 does not show us the effect of the pore boundary area clearly, so a quantitative study of the pore boundary area effect should be carried out.

If we divide a single large pore into several small pores, the boundary area will be expanded significantly, even the porosity keeps fixed. In this study, the porosity keeps at $\Phi = 0.36$, and the single pore as shown in Fig. 4(a) is divided uniformly into 4, 9, 16, and 25 small pores, respectively. Here, we introduce a normalized parameter A/A_0 to reflect the expansion of the scattering boundary area, where $A_0 = 2L$ denotes the boundary area of the pure thin film, and $A = 2L + 4nD$ is the total boundary area of the nano-porous thin film, where D is the pore size, like the definition of the single pore in Fig. 4(a), and n is the number of nanopores.

The boundary conditions in this section are the same as those in the single pore film. By solving the PBTE, we obtain the temperature fields as shown in Fig. 6. With the increase of the pore number, the boundary area is expanded, and the phonon scattering on the boundaries is enhanced. Compared with the pure thin film as presented in Fig. 6(a), it is more easily for a low-temperature zone to appear behind each pore, indicating a reduction in heat transfer. In addition, if we continuingly increase the number of pores, the area of the low-temperature zone will be expanded further, and finally the heat transfer will be significantly blocked.

Figure 7 shows the effective thermal conductivity of the nano-porous thin film against the pore boundary area at a fixed porosity $\Phi = 0.36$. We can see that as the boundary area increases, the thermal conductivity decreases gradually. The effect of specularity p is more important when the pore

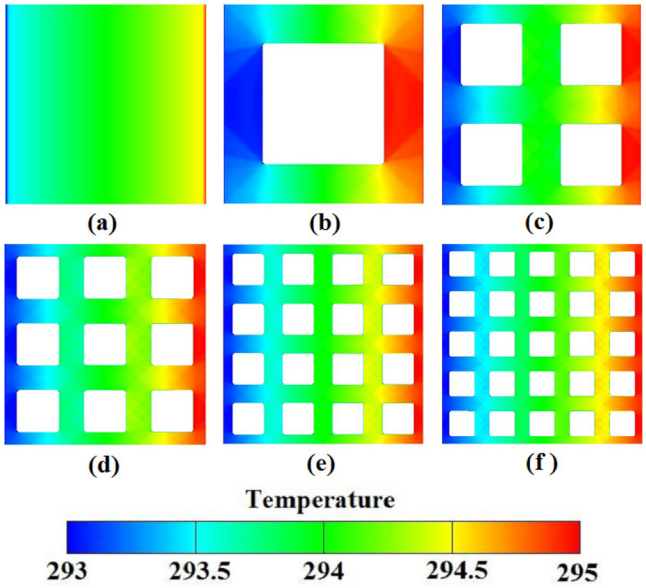

FIG. 6. Temperature fields of nano-porous silicon thin film ($p = 0.0$).

boundary area gets larger. Once the scattering boundary area is expanded more than twice of the pure thin film, λ will be reduced at least about one third of the thermal conductivity of the pure thin film, and for $p = 0.0$ the thermal conductivity can be reduced more as we increase the value of A/A_0. For example, when the boundary area is expanded seven times (i.e., $A/A_0 = 7$), compared with the pure thin film, λ can be reduced by about 4–9 times for $p = 0.0$, while it can still be reduced by about 2–4 times for $p = 1.0$. Compared with the porosity, the above analysis demonstrates that the pore boundary area (or specific surface area) does have more important effect on the thermal conductivity of the porous thin film.

C. Discussion of relation between heat flux and thermal conductivity

In this section, we study the heat flux field to discuss the reduction of the effective thermal conductivity of the nano-porous thin film. According to Eq. (13), as long as the heat transfer is treated as one-dimensional thermal conduction, the x-direction component of the heat flux (q_x) is dominant to the effective thermal conductivity. Therefore, the reduction of the effective thermal conductivity can be focused on reducing q_x. The relation between q_x and the total heat flux $|\mathbf{q}|$ is expressed as

$$q_x = |\mathbf{q}|\cos\theta = \sqrt{q_x^2 + q_y^2}\cos\theta, \tag{16}$$

where θ is the angle between the directions of q_x and $\mathbf{q}$. From Eq. (16), we can know that a larger θ leads to a lower q_x and thus the thermal conductivity. By studying the distribution of θ, we can recognize how much the local heat flux q_x can affect the effective thermal conductivity of the nanoporous thin film, and we can also explain how the pore structure and pore placement affect the thermal conduction in the nanoporous thin film. For example, Song and Chen[34] reported that the thermal conductivity of porous thin film is insensitive to the pore alignment. But from their experimental data, we can distinguish that the thermal conductivity of the aligned pore thin film (SOI-10 A sample) is slightly higher than that of the staggered pore thin film (SOI-10 S sample). It is difficult to explain this phenomenon if only analyzing the temperature field, but we can do it if studying the θ distribution. Here, we use two constructed porous thin films, see Fig. 8. In the simulation, the dimensionless film thickness is fixed at $\mathrm{Kn} = \Lambda_{\mathrm{bulk}}/L = 1.0$, and the corresponding boundary conditions and parameters are the same as those in Sec. III A. From Fig. 8, we can see that the zone of the high θ region in the staggered pore film is broader than that in the aligned pore film, which denotes that the staggered pores can disorder the local heat flux q_x more significantly. The average angle of $\bar{\theta}$ over the whole simulated zone is also calculated. We have $\bar{\theta} = 49.4°$ for the simulated staggered pore with $\lambda = 10.02$ W/(m K) while $\bar{\theta} = 44.0°$ for the aligned pore with $\lambda = 11.75$ W/(m K).

Most importantly, we can artificially change the pore placement of the porous thin film to increase the value of θ

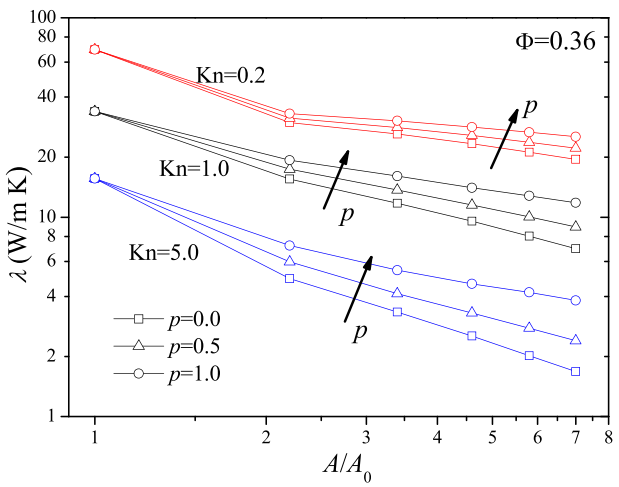

FIG. 7. Effect of scattering boundary area on effective thermal conductivity (cross-plane) at $\mathrm{Kn} = 0.2$, $\mathrm{Kn} = 1.0$, and $\mathrm{Kn} = 5.0$. $A/A_0 = 1$ denotes the pure thin film.

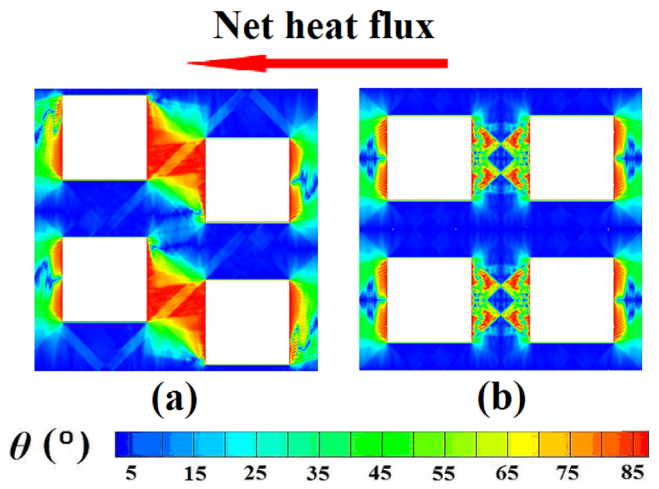

FIG. 8. Distribution of θ in the staggered and aligned porous thin film (cross-plane). (a) Staggered pore with $\lambda_{(a)} = 10.02$ W/(m K) and $\bar{\theta}_{(a)} = 49.4°$. (b) Aligned pore with $\lambda_{(b)} = 11.75$ W/(m K) and $\bar{\theta}_{(b)} = 44.0°$.

for the reduction of the effective thermal conductivity according to Eqs. (13) and (16). An example is demonstrated to describe the active design of the structure of the nano-porous thin film at Kn = 1.0 and $p = 0.0$.

(1) To reduce the thermal conductivity, we should disturb θ field for increasing the value of θ in the pure thin film. We open a pore in the centre of the film, and solve the θ distribution as shown in Fig. 9(a).
(2) To increase the value of θ further, we open pores in the small-θ zones, i.e., on the bottom and top of the centre pore, and the updated θ field is shown in Fig. 9(b) and we have $\lambda_{(b)} = 7.42$ W/(m K) compared with $\lambda_{(a)} = 21.01$ W/(m K). Note that, do not arrange pores in large-θ zones, such as in the downstream and upstream of the centre pore as shown in Fig. 9(c), which cannot disorder the θ distribution as effective as that in Fig. 9(b). The corresponding calculated thermal conductivity is $\lambda_{(c)} = 20.62$ W/(m K) compared with $\lambda_{(b)} = 7.42$ W/(m K) at the same porosity and specific surface area.
(3) If possible, we can arrange more pores in the small-θ zones to get a further reduction of the thermal conductivity, such as the small pores in the four corners of the film, see Fig. 9(d). We have a lower thermal conductivity $\lambda_{(d)} = 6.31$ W/(m K). The calculated average angle over the whole zone is $\bar{\theta}_{(a)} = 35.8^\circ < \bar{\theta}_{(c)} = 38.1^\circ < \bar{\theta}_{(b)} = 44.6^\circ < \bar{\theta}_{(d)} = 49.0^\circ$, which also accords with the relation between thermal conductivity and angle of heat fluxes. Note that, when arrange pores in the thin film, we should avoid too small spacing between adjacent pores, because the small spacing will enhance the electron scattering on the pore boundaries, and then result in a reduction of the electrical conductivity of thin film.

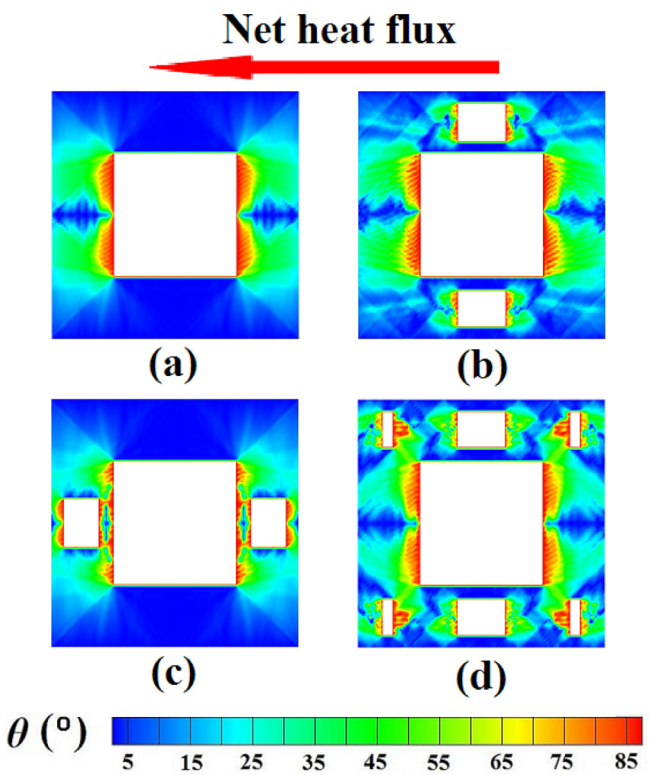

FIG. 9. Active design for structure of nano-porous thin film (cross-plane). (a) $\lambda_{(a)} = 21.01$ W/(m K) and $\bar{\theta}_{(a)} = 35.8^\circ$. (b) $\lambda_{(b)} = 7.42$ W/(m K) and $\bar{\theta}_{(b)} = 44.6^\circ$. (c) $\lambda_{(c)} = 20.62$ W/(m K) and $\bar{\theta}_{(c)} = 38.1^\circ$. (d) $\lambda_{(d)} = 6.31$ W/(m K) and $\bar{\theta}_{(d)} = 49.0^\circ$.

From the above analysis, we can believe that solving and analyzing the local angle field between heat fluxes can serve as an active tool to optimize the structures of the nano-porous thin film, especially to arrange the pores reasonably and avoid processing pores randomly. The present method can also be applied to analyze the effect of pore shape on the thermal conductivity, such as triangular, circle, and hexagonal pores, and even it is also straightforward to extend for designing complex 2-D or 3-D structures for the porous media since the method of solving θ distribution according to Eq. (16) is universal.

IV. CONCLUSIONS

We have solved the Phonon Boltzmann Transport Equation based on the phonon frequency-dependent model by using the Discrete Ordinates Method to numerically study the effective thermal conductivity of nano-structured silicon thin film with pores. The porosity and film thickness have significant effect on the thermal conductivity. As the porosity increases and the film thickness decreases, the thermal conductivity gets lower. When the Knudsen number rises up to 10 and the porosity up to 64%, we can get an extremely low thermal conductivity reduced by two orders of magnitude compared with the bulk value. Phonon scattering on the boundaries is crucial to reduce the thermal conductivity, and it is quite useful to expand the boundary area to enhance the phonons scattering. The θ angle method (the angle between the directions of q_x and **q**) has been proposed to analyze the effect of nano-pore placement, and the results demonstrate that the θ angle method is quite useful to optimize the porous structure of nano-porous thin film.

ACKNOWLEDGMENTS

This work was supported by the National Natural Science Foundation of China under Grant Nos. 51076125 and 51222604.

[1]G. Chen, M. S. Dresselhaus, G. Dresselhaus, J. P. Fleurial, and T. Caillat, Int. Mater. Rev. **48**, 45 (2003).
[2]M. S. Dresselhaus, G. Chen, M. Y. Tang, R. G. Yang, H. Lee, D. Z. Wang, Z. F. Ren, J. P. Fleurial, and P. Gogna, Adv. Mater. **19**, 1043 (2007).
[3]R. Venkatasubramanian, E. Silvona, T. Colpitts, and B. O'Quinn, Nature **413**, 597 (2001).
[4]A. Majumdar, Science **303**, 777 (2004).
[5]G. J. Snyder and E. S. Toberer, Nature Mater. **7**, 105 (2008).
[6]L. E. Bell, Science **321**, 1457 (2008).
[7]H. J. Golsmid, *Thermoelectric Refrigeration* (Plenum, New York, 1964).
[8]G. Chen, *Nanoscale Energy Transport and Conversion, A Parallel Treatment of Elections, Molecules, Phonons, and Photons* (Oxford University Press, London, 2005).
[9]B. Feng, Z. X. Li, and X. Zhang, J. Appl. Phys. **105**, 104315 (2009).
[10]B. Feng, Z. X. Li, and X. Zhang, Thin Solid Films **517**, 2803 (2009).
[11]P. P. Zhang, E. Tevaarwerk, B. N. Park, D. E. Savage, G. K. Celler, I. Knezevic, P. E. Evans, M. A. Eriksson, and M. G. Lagally, Nature **439**, 703 (2006).
[12]J. K. Yu, S. Mitrovic, D. Tham, J. Varghese, and J. R. Heath, Nat. Nanotechnol. **5**, 718 (2010).
[13]L. C. Liu and M. J. Huang, Int. J. Therm. Sci. **49**, 1547 (2010).

[14]H. Lee, D. Vashaee, D. Z. Wang, M. S. Dresselhaus, Z. F. Ren, and G. Chen, J. Appl. Phys. **107**, 094308 (2010).
[15]J. Fang, C. B. Kang, Y. Huang, S. H. Tolbert, and L. Pilon, J. Phys. Chem. C **116**, 12926 (2012).
[16]K. Miyazaki, S. Tanaka, and D. Nagai, ASME J. Heat Transfer **134**, 051018 (2012).
[17]G. Romano, A. D. Carlo, and J. C. Grossman, J. Comput. Electron **11**, 8 (2012).
[18]Z. M. Zhang, *Nano/Microscale Heat Transfer* (McGraw-Hill, New York, 2007).
[19]A. Majumdar, ASME J. Heat Transfer **115**, 7 (1993).
[20]G. Chen and C. L. Tien, J. Thermophys. Heat Transfer **7**, 311 (1993).
[21]Q. Hao, G. Chen, and M. S. Jeng, J. Appl. Phys. **106**, 114321 (2009).
[22]A. S. Henry and G. Chen, J. Comput. Theor. Nanosci. **5**, 141 (2008).
[23]A. Ward and D. A. Broido, Phys. Rev. B **81**, 085205 (2010).
[24]E. Pop and R. W. Dutton, J. Appl. Phys. **96**, 4998 (2004).
[25]M. Asheghi, K. Kurabayashi, R. Kasnavi, and K. E. Goodson, J. Appl. Phys. **91**, 5079 (2002).
[26]R. G. Yang and G. Chen, Phys. Rev. B **69**, 195316 (2004).
[27]M. F. Modest, *Radiative Heat Transfer*, 2nd ed. (Academic Press, Elsevier Science, USA, 2003).
[28]J. D. Chung and M. Kaviany, Int. J. Heat Mass Transfer **43**, 521 (2000).
[29]S. Volz, D. Lemonnier, and J. B. Saulnier, Microscale Thermophys. Eng. **5**, 191 (2001).
[30]D. P. Sellan, J. E. Turney, A. J. H. McGaughey, and C. H. Amon, J. Appl. Phys. **108**, 113524 (2010).
[31]J. Fang, C. Reitz, T. Brezesinski, E. J. Nemanick, C. B. Kang, S. H. Tolbert, and L. Pilon, J. Phys. Chem. C **115**, 14606 (2011).
[32]T. Coquil, E. K. Richman, N. J. Hutchinson, S. H. Tolbert, and L. Pilon, J. Appl. Phys. **106**, 034910 (2009).
[33]T. Y. Hsieh, H. Lin, T. J. Hsieh, and J. C. Huang, J. Appl. Phys. **111**, 124329 (2012).
[34]D. Song and G. Chen, Appl. Phys. Lett. **84**, 687 (2004).